# 行政院國家科學委員會專題研究計畫　期中精簡報告

## 有限長度之圓柱形粒子在圓柱管中之電泳(1/3)

計畫類別：個別型計畫
計畫編號：NSC91-2214-E-002-014-
執行期間：91 年 08 月 01 日至 92 年 07 月 31 日
執行單位：國立臺灣大學化學工程學系暨研究所

計畫主持人：徐治平

報告類型：精簡報告

處理方式：本計畫可公開查詢

中　華　民　國 92 年 5 月 7 日

## 計畫執行概要

本計畫目前進展順利，已完成主要的理論推導、主控方程式的求解、及相關之數值模擬與分析。後附資料爲目前已獲得之部份結果。

**摘 要**

本研究中，我們進一步探討周圍存在的邊界對一膠體粒子電泳的影響。典型的例子包括有，粒子在一狹窄空間如孔洞中或是在高濃度懸浮系統中的電泳行爲。文中考慮一有限長度，帶電之非導電性圓柱形粒子在一未帶電的無窮圓柱管中，沿管中心移動之電泳行爲。文中我們限制該系統是低電位的情形，而主要探討參數有：粒子幾何形狀比(粒子半徑/粒子長度)、粒子的表面帶電情況與電雙層厚度。我們發現圓柱形粒子受電場驅動而移動的方向是決定於該圓柱形粒子側 面表面帶電符號。圓柱形粒子電泳度隨 $\lambda$(圓柱形粒子半徑/無窮圓柱管管徑)的變化則會隨粒子上下兩面與側面的帶電性符號相同或相異有明顯不同變化趨勢。帶均勻表面電荷密度之圓柱形粒子，電泳度會隨著 $\lambda$ 的變化有一最大值存在。粒子上下兩面與側面帶相反電性電荷時，電泳度會隨 $\lambda$ 增加而呈單調函數減少。我們也發現圓柱形粒子在圓柱管中的電泳度會隨該粒子幾何形狀變的越瘦長(粒子幾何形狀比越小)而增加。圓柱管管壁對粒子所造成的邊界效應則是隨著粒子所帶表面電荷密度的增加而益加顯著。

## 1. INTRODUCTION

Electrophoresis is one of the most widely adopted analytical tools in the study of the surface properties of colloidal particles. It also plays an important role in both biochemistry and biophysics when purification and characterization of biochemical materials are involved. Apparently, a detailed understanding of the electrophoretic behavior of a colloidal particle is essential to both fundamental theory and applications. The analysis of thisproblem, however, is not an easy task. This is mainly due to the complicated interaction between hydrodynamic and electric effects, and the governing equations involved are coupled nonlinear differential equations. Smoluchowski [1] derived the following relation between the electrophoretic velocity $\boldsymbol{U}$ of an isolated, nonconducting, charged particle in an infinite electrolyte solution of viscosity $\eta$ and permittivity $\varepsilon$ and an applied field $\boldsymbol{E}$:

$$\boldsymbol{U} = \frac{\varepsilon \zeta \boldsymbol{E}}{\eta}$$

where $\zeta$ is the zeta potential of the particle. This expression is applicable to particle of arbitrary shape, provided that its local radius of curvature is much larger than the thickness of the double layer surrounding it [2]. The ratio $\boldsymbol{U}/\boldsymbol{E}$ is known as the electrophoretic mobility of the particle.

In many applications of electrophoresis, colloidal particles are not isolated, and they move under the influence of neighboring particles or the presence of boundaries. Typical example for the former includes the electrophoresis of a concentrated dispersion where the interaction between neighboring particles is significant, and that for the latter includes the electrophoresis through a pore in a membrane which occurs in electrophoretic separation of proteins. Modification of Smoluchowski equation to

take these effects into account is necessary from practical point of view. Relevant studies are ample in the literature. Most of them, however, are based on entities of one-dimensional nature such as sphere [1-22] and infinite cylinder [23-28]. Note that in the latter the end effect of a particle is neglected. For particles of other shapes [29-34] the electrokinetic calculations are usually complicated and time consuming, and therefore, most of the relevant works are based on the assumption of thin double layer [4-11,13,15,16,26,27,29,30,32,33]. In this case the solution procedure for the electric field can be simplified dramatically. In practice, colloidal particles can assume arbitrary geometry[1], and extension of previous analyses to a more general case is highly desirable. Another important factor is the non-homogeneous nature of the charged conditions on particle surface. The charge on the basal plane of a kaolin particle, for instance, can have a different sign than that on its facial plane. Including this effect in the relevant analysis seems to be realistic.

In this study we consider the electrophoresis of a finite, non-uniformly charged, nonconducting cylindrical particle with a moderate thick electrical double layer. Several specific shapes can be simulated by adjusting the aspect ratio of the particle. For example, it may represent a plate-like particle such as montmorillonite with a nonuniform surface charge distribution. The boundary effects are also examined by considering the case where the particle is moving along the axis of cylindrical pore.

## 2. THEORY

The space charge density of an electrolyte solution containing ionic species of number density $n_i$ and valence $z_i$ is

$$\rho = \sum_i e z_i n_i$$

(2)

where $e$ is the elementary charge. Suppose that the electrical potential $\Psi$ can be described by Poisson's equation,

$$\nabla^2\Psi = -\frac{\rho}{\varepsilon}$$

where $\varepsilon$ is the permittivity of the electrolyte solution. At steady state, the distribution of the ions can be described by the conservation equation,

$$\nabla\cdot\left[n_i\boldsymbol{u} - D_i\left(\nabla n_i + \frac{ez_i n_i}{k_B T}\nabla\Psi\right)\right] = 0 \qquad (4$$

where $\nabla$ is the gradient operator, $D_i$ is the diffusivity of ions of species $i$, $k_B$ is the Boltzmann constant, $T$ is the absolute temperature and $\boldsymbol{u}$ is the fluid velocity. We assume that the flow field can be described by the Navier-Stokes equation in the creeping flow regime

$$\eta\nabla^2\boldsymbol{u} - \nabla p = \rho\nabla\Psi$$

$$\nabla\cdot\boldsymbol{u} = 0$$

where $\eta$ is the fluid viscosity and $p$ is the pressure. The term on the right-hand side of Eq. (5) denotes the electrical body force. For simplicity, we consider an incompressible fluid with constant physical properties.

Referring to Fig.1, we consider a rigid, nonconducting, cylindrical particle of radius $a$ and length $2d$ on the axis of an infinite cylindrical pore of radius $b$ filled with an electrolyte solution. Since the length of the particle is comparable to its radius, the end effect of the top and bottom surfaces of the particle can be significant. A uniform electric field $\boldsymbol{E}$ in the direction along the axis of the cylindrical pore is applied, and the particle moves along the axis of the pore, that is, an axisymmetric problem is considered. Let $\sigma_1$ be the charge density on the top and bottom surfaces of the particle and $\sigma_2$ be that on the lateral surface. The cylindrical coordinates are chosen with its origin located at the center of the particle. As illustrated in Fig.5.1b, the axisymmetric nature of the geometry adopted suggests that only the $(r, z)$ domain needs to be considered.

**2.1. Electrical Field**

Following Henry's[35] classic treatment, we assume that the electrical potential $\Psi$ can be expressed as a linear superposition of the electrical potential in the absence of the applied electric field (i.e., equilibrium potential, $\Psi_1$), and the electrical potential outside the particle that arises from the applied field, $\Psi_2$. This assumption is valid under conditions where the applied electric field is weak relative to the electric fields induced by the particle. This implies that the ionic cloud surrounding the particle is only slightly distorted by the applied electric field, that is, the effect of double layer polarization is negligible. Therefore, the ionic concentrations can be assumed to attain their equilibrium distributions, which can be obtained from Eq. (4) by letting $\boldsymbol{u}=\boldsymbol{0}$. It can be shown that

$$n_i = n_{i0}\, exp\left(\frac{-ez_i\Psi_1}{k_BT}\right)$$

(7)

where $n_{i0}$ is the bulk number density of ionic species $i$. If the electrical potential is low, Debye-Hückel approximation is applicable, and $\Psi_1$ can be described by

$$\nabla^2 \Psi_1 = \kappa^2 \Psi_1$$

where the inverse Debye length or Debye-Hückel parameter $\kappa$ is defined by

$$\kappa = \left( \frac{e^2 \sum_i z_i^{\,2} n_{io}}{\varepsilon \, k_B T} \right)^{1/2}$$

Similarly, the electrical potential associated with the applied electric field $\Psi_2$ can be described by

$$\nabla^2 \Psi_2 = 0$$

The boundary conditions associated with Eqs (8) and (10) are assumed as

$$\boldsymbol{n} \cdot \nabla \Psi_1 = \frac{-\sigma_1}{\varepsilon}, \quad \frac{\partial \Psi_2}{\partial z} = 0, \quad |z| = d, \quad 0 \le r \le a \qquad (11)$$

$$\boldsymbol{n} \cdot \nabla \Psi_1 = \frac{-\sigma_2}{\varepsilon}, \quad \frac{\partial \Psi_2}{\partial r} = 0, \quad r = a, \quad -d \le z \le d \qquad (12)$$

$$\boldsymbol{n} \cdot \nabla \Psi_1 = 0, \quad \frac{\partial \Psi_2}{\partial r} = 0, \quad r = b \qquad (13)$$

$$\Psi_1 = 0, \quad \nabla\Psi_2 = -\boldsymbol{E}, \quad |z| \to \infty, \quad r < b \tag{14}$$

In these expressions $\boldsymbol{n}$ is the unit normal directed into the liquid phase.

**2.2. Flow Field**

The axisymmetric nature of the problem under consideration and the charged conditions on particle surface implies that it will move in the direction of the applied electric field, the particle moves in the direction of the applied electric field and the torque it experienced vanishes. The governing equations for the electric and flow fields can be decoupled by expanding each dependent variables in a double perturbation series in $E$ and $\zeta$, and neglecting all the nonlinear terms [17,20]. It can be shown that Eqs (5) and (6) become

$$\eta\nabla^2\boldsymbol{u}^{(1,1)} - \nabla p^{(1,1)} = \rho^{(0,1)}\nabla\Psi^{(1,0)} \tag{15}$$

$$\nabla\cdot\boldsymbol{u}^{(1,1)} = 0$$

where $\rho^{(0,1)} = -\varepsilon\kappa^2\Psi_1$, $\Psi^{(1,0)} = \Psi_2$, and the superscripts denote the order in $(E,\zeta)$ of the quantity. The boundary conditions associated with these equations are assumed as

$$\boldsymbol{u} = U\boldsymbol{i}_z \quad \text{on particle surface} \tag{17}$$

$$\boldsymbol{u} = 0, \quad r = b$$

$$\boldsymbol{u} = 0, \quad |z| \to \infty, \quad r < b$$

where $\boldsymbol{i}_z$ is the unit vector in $z$-direction. Equations (17) and (18) arise from the no-slip condition on both particle surface and pore wall.

### 2.3. Electrophoretic Mobility

The total force acting on the particle comprises the hydrodynamic force and the electrostatic force. The axisymmetric nature of the problem under consideration suggests that only the forces in $z$-direction need to be evaluated. The electrostatic force experienced by the particle in the z-direction can be calculated by

$$F_E^Z = \iint_S \sigma^{(0,1)} E_Z^{(1,0)} dS = \iint_S \sigma^{(0,1)} \left(-\frac{\partial \Psi^{(1,0)}}{\partial z}\right) dS \qquad (20)$$

where $S$ denotes the surface of the particle. The hydrodynamic force acting on the particle in the $z$-direction, $F_D^Z$, can be decomposed into two terms: that arises from the viscous force, $F_{DV}^Z$, and that arises from the hydrodynamic pressure, $F_{DP}^Z$, that is,

$$F_D^Z = F_{DV}^Z + F_{DP}^Z$$

$F_{DV}^Z$ and $F_{DP}^Z$ can be calculated respectively by

$$F_{DV}^Z = \iint_S \eta \frac{\partial (\boldsymbol{u} \cdot \boldsymbol{t})}{\partial n} t_z dS$$

$$F_{DP}^{Z} = \iint_{S} -pn_z dS$$

where $\boldsymbol{t}$ is the tangential unit vector on particle surface, and $t_z$ and $n_z$ are respectively the $z$-component of $\boldsymbol{t}$ and $\boldsymbol{n}$. The mobility of the particle can be calculated based on the fact that the total force acting on it vanishes at steady state, that is,

$$F_{D}^{Z} + F_{E}^{Z} = 0$$

## 3. RESULTS AND DISCUSSIONS

The behavior of the system under consideration is examined through numerical simulation. The governing equations and the associated boundary conditions are solved by FlexPDE [36], a partial differential solver based on a finite element method, on an IBM-PC compatible machine. The solution procedure is summarized in the following steps. Step 1, Solve Eqs (8) and (10) subject to boundary conditions, Eqs (11)-(14), for the electric potentials $\Psi_1$ and $\Psi_2$, and calculate the electrostatic force $F_E^Z$ by Eq. (20). Step 2, substituting $\Psi_1$ and $\Psi_2$ into Eq. (15) and solving the resultant equation simultaneously with Eq. (16) [37] with an initially guessed velocity $U$ to evaluate $\boldsymbol{u}$ and $p$. The hydrodynamic forces $F_{DV}^Z$ and $F_{DP}^Z$ are then calculated by Eqs (22) and (23). If Eq. (24) is satisfied, then the solution procedure is completed. Otherwise, go to the next step. Step 3, a new value for $U$ is assumed back to step 2. In step 2, the criterion $\left|(F_E^Z + F_D^Z)/F_E^Z\right| \le 0.5\%$ is adopted to determine if Eq. (24) is satisfied. The applicability and accuracy of the software used are checked by comparing with the available results in the literature. Since we fail to find a system, which match exactly with our problem, the results for the

electrophoresis of a sphere along the axis of a cylindrical pore examined by Ennis and Anderson [17] and Shugai and Carnie [20] are adopted [17,20]. The former solved the problem based on a reflection method, and the latter solved it numerically. Fig.2 shows the results based on these approaches and that based on our approach. Shugai and Carnie [20], concluded that, due to numerical error, their numerical approach was inappropriate for small $\lambda$ (ratio of particle radius to pore radius). On the other hand, due to the overlap of double layers, the reflection method might not provide accurate results if $\lambda$ is large. Fig.2 reveals that our approach does not have these limitations, and seems to work well for the range of $\lambda$ considered.

Fig.3 shows the variation of the scaled electrophoretic mobility of a particle $\mu^*$ as a function of $\lambda$ ($=a/b$) for various particle aspect ratio $a/d$ and $\kappa a$. Here, the surface of the particle is uniformly charged. Fig.3 reveals that the smaller the $\kappa a$ (thicker double layer) the smaller the $\mu^*$. This is because if the double layer is thick, the influence of the electric body force is capable of reaching a deep region in the liquid phase. Fig.3 also indicates that $\mu^* \to 0$ as $\lambda \to 1$. This is expected since $\lambda \to 1$ implies that the particle attaches the wall of the pore. The trend in Fig.3a and 3b that $\mu^*$ decreases with the increase in $\lambda$ is similar to that for the case of a sphere in a cylindrical pore [17,20]. It is interesting to note, however, that if $a/d$ is large, $\mu^*$ may exhibit a local maximum as $\lambda$ varies as illustrated in Fig.3c-3e which is not observed for the corresponding sphere in cylindrical problem.

The variations of the scaled electrophoretic mobility of a particle $\mu^*$ as a function of $\lambda$ for various particle aspect shapes $a/d$ and $\kappa a$ are illustrated in Fig.4. Here, the surface of the particle is nonuniformly charged. As can be seen from Fig.4, $\mu^*$ increases with the increase in $\kappa a$, but decreases with the increase in $\lambda$ as expected. Note that the local maximum of $\mu^*$ as $\lambda$ varies shown in Fig.3 does

not appear in the present nonuniformly charged condition. This implies that the direction of the translational motion of a particle is dominated by sign of the charge on its lateral surface: if $\sigma_2 > 0$, the particle moves in the direction of applied electric field, and the reverse is true if $\sigma_2 < 0$. On the other hand, the magnitude of the mobility of a particle is influenced mainly by the sign of the charge on its top and bottom surface.

Fig.5 shows the variation of the scaled electrophoretic mobility of a particle $\mu^*$ as a function of $\lambda$ for the case of Fig.3. It reveals that the larger the $a/d$ the smaller the scaled electrical mobility $\mu^*$. Fig.5 indicates that as $a/d$ increases, the value of $\lambda$ at which the local maximum of $\mu^*$ occurs shifts to a larger value, and the shape of $\mu^*$ against $\lambda$ curve becomes flatter. Also, the larger the $\kappa a$, the smaller the value of $a/d$ needed to observe the local maximum in $\mu^*$. Fig.5 also suggests that for fixed $\kappa a$, while the difference in the $\mu^*$ between various particle aspect ratios is appreciable as $\lambda \to 0$, it becomes inappreciable as $\lambda \to 1$. That is, the effect of boundary (pore wall) on the electrophoretic behavior of a particle depends on its shape; the closer the particle radius to pore radius the less the difference between the behaviors of particles of different shapes.

Fig.6 shows the variation of the scaled electrophoretic mobility of a particle $\mu^*$ as a function of its aspect ratio $a/d$ for various $\kappa a$ at two different charged conditions on particle surface. This figure indicates that, for a fixed $\kappa a$, $\mu^*$ decreases with the increase in $a/d$, in general. Note that, if $\kappa a$ is small, the effect of the charged conditions on particle surface on $\mu^*$ is insignificant. However, if $\kappa a$ is large, $\mu^*$ becomes sensitive to the charged conditions on particle surface. In this case the mobility of a particle with its lateral surface and top and bottom surfaces carry different charges is larger than that of a uniformly charged particle. Note that as $a/d \to 0$ (i.e., infinitely long particle), the effect of the charged conditions on

particle surface on $\mu^*$ becomes insignificant again.

Fig.7 shows the variation of the scaled electrophoretic mobility of a particle $\mu^*$ as a function of $\lambda$ for various types of charged conditions and particle aspect ratio *a/d*. This figure reveals that $\mu^*$ increases with the increase in the charge density on particle surface, as expected. According to Fig.7, it seems that the occurrence of the local maximum in $\mu^*$ as $\lambda$ varies is independent of the level of the charge density on a particle; it depends largely on its shape. Fig.7 also suggests that the lower the charge density, the less sensitive the variation of $\mu^*$ as $\lambda$ varies.

Fig.8 illustrates the variation of the scaled electrophoretic mobility of a particle $\mu^*$ as a function of its surface charge density for the case of Fig.3 at various particle aspect ratio *a/d* at two different charged conditions on particle surface. For illustration, we assume $|\sigma_1| = |\sigma_2|$. Fig.8 reveals that the mobility of a particle is roughly, positively linearly dependent on it surface charge density. Also, the mobility of a particle with it lateral surface and top and bottom surfaces oppositely charged is larger than that of a uniformly charged particle. This is consistent with the results shown in Fig.6.

**REFERENCES**


[1] Hunter, R. J.,"Foundations of Colloid Science", Vol. I. Clarendon Press, Oxford, 1989.

[2] Morrison, F. A., *J. Colloid Interface Sci.* **34**, 210 (1970).

[3] O'Brien, R. W., and White, L. R., *J. Chem. Soc. Faraday Trans2* **74**, 1607 (1978).

[4] O'Brien, R. W., and Hunter, R. J., *Can. J. Chem.* **59**, 1878 (1981)

[5] Ohshima, H., Healy, T. W., and White, L. R., *J. Chem. Soc. Faraday Trans. 2* **79**, 1613 (1983).

[6] O'Brien, R. W., *J. Colloid Interface Sci.* **92**, 204 (1983).

[7] Keh, H. J., and Anderson, J. L., *J. Fluid Mech.* **153**, 417 (1985).

[8] Anderson, J. L., *J. Colloid Interface Sci.* **105**, 45 (1985).

[9] Keh, H. J., and Chen, S. B., *J. Fluid Mech.* **194**, 377 (1988).

[10] Keh, H. J., and Lien, L. C., *J. Chinese Inst. Chem. Engrs* **20**, 283 (1989).

[11] Keh, H. J., and Lien, L. C., *J. Fluid Mech.* **224**, 305 (1991).

[12] Yoon, B. J., *J. Colloid Interface Sci.* **142**, 575 (1991).

[13] Solomentsev, Y. E., Pawav, Y., and Anderson, J. L., *J. Colloid Interface Sci.* **158**, 1 (1993).

[14] Zydney, A. L., *J. Colloid Interface Sci.* **169**, 476 (1995).

[15] Keh, H. J., and Chiou, J. Y., *AIChE J.* **42**, 1397 (1996).

[16] Keh, H. J., and Jan, J. S., *J. Colloid Interface Sci.* **183**, 458 (1996).

[17] Ennis, J., and Anderson, J. L., *J. Colloid Interface Sci.* **185**, 497 (1997).

[18] Lee, E., Chu, J. W., and Hsu, J. P., *J. Colloid Interface Sci.* **196**, 316 (1997).

[19] Lee, E., Chu, J. W., and Hsu, J. P., *J. Colloid Interface Sci.* **205**, 65 (1998).

[20] Shugai, A. A., and Carnie, S. L., *J. Colloid Interface Sci.* **213**, 298 (1999).

[21] Ohshima, H., *J. Colloid Interface Sci.* **239**, 587 (2001).

[22] Chu, J. W., Lin, W. H., Lee, E., and Hsu, J. P., *Langmuir* **17**, 6289 (2001).

[23] Stigter, D., *J. Phys. Chem*. **82**, 1417 (1978).

[24] Stigter, D., *J. Phys. Chem*. **82**, 1424 (1978).

[25] Sherwood, J. D., *J. Chem. Soc. Faraday Trans*. *2* **78**, 1091 (1982).

[26] Keh, H. J., Horng, K. D., and Kuo, J. *J. Fluid Mech.* **231**, 211 (1991).

[27] Keh, H. J., and Chen, S. B., *Langmuir* **9**, 1142 (1993).

[28] Chen, S. B., and Koch, D. L., *J. Colloid Interface Sci.* **180**, 466 (1996).

[29] O'Brien, R. W., and Ward, D. N., *J. Colloid Interface Sci.* **121**, 402 (1988).

[30] Fair, M. C., and Anderson, J. L., *J. Colloid Interface Sci.* **127**, 388 (1989).

[31] Yoon, B. J., and Kim, S., *J. Colloid Interface Sci.* **128**, 275 (1989).

[32] Keh, H. J., and Huang, T. Y., *J. Colloid Interface Sci.* **160**, 354 (1993).

[33] Feng, J. J., and Wu, W. Y., *J. Fluid Mech.* **264**, 41 (1994).

[34] Sherwood, J. D., and Stone, H. A., *Phys. Fluid.* **7**, 697 (1995).

[35] Henry, D. C., *Proc. R. Soc. Lond.* A **133**, 106 (1931).

[36] FlexPDE version 2.22, PDE Solutions Inc., USA.

[37] Backstrom, G., "Fluid Dynamics by Finite Element Analysis." Studentlitteratur, Sweden, 1999.

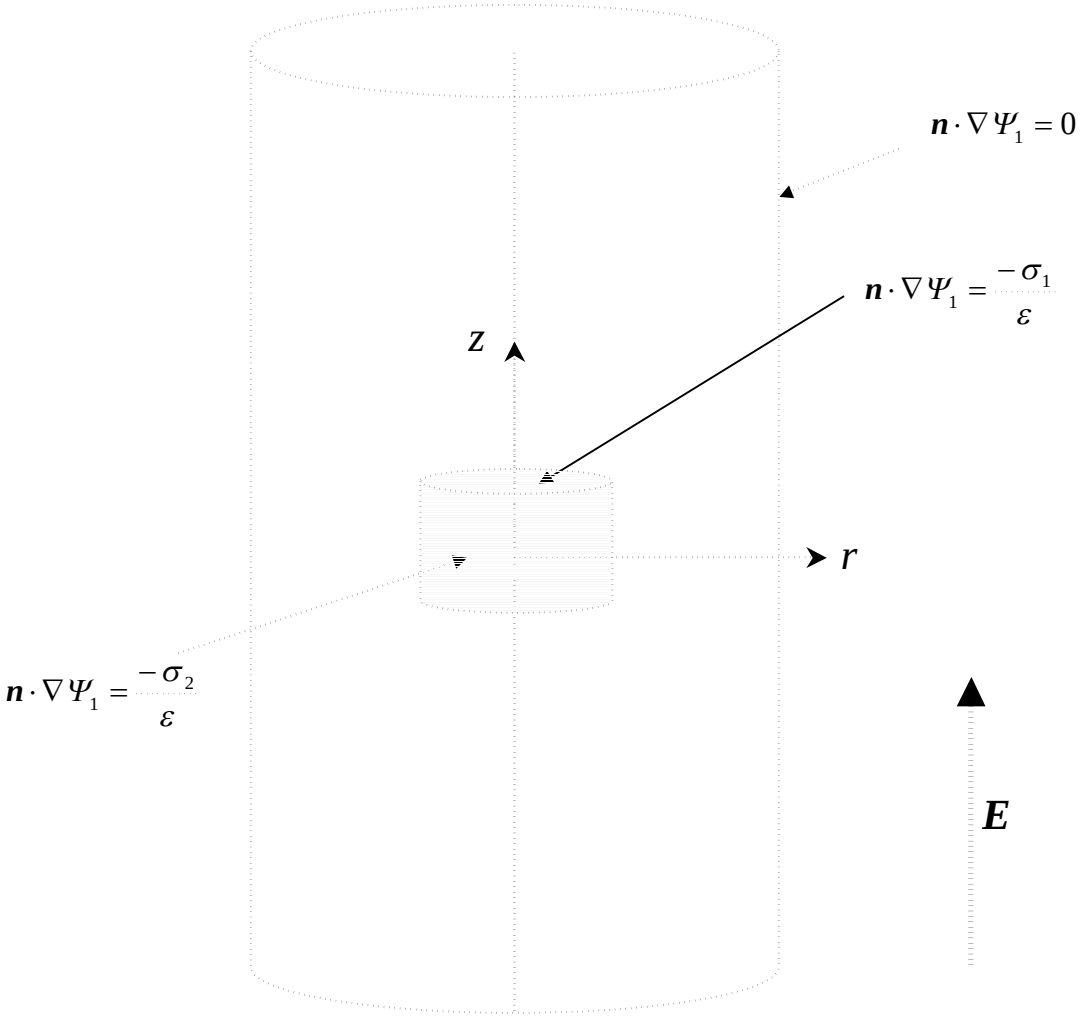


Fig.1a. Schematic representation of the problem considered. (A charged cylindrical particle is placed on the axis of an uncharged infinite cylindrical pore. An electric field ***E*** parallel to the axis of the pore is applied. $\sigma_1$ is the charge density on the top and bottom surfaces of the particle, and $\sigma_2$ is that on the lateral surface.)

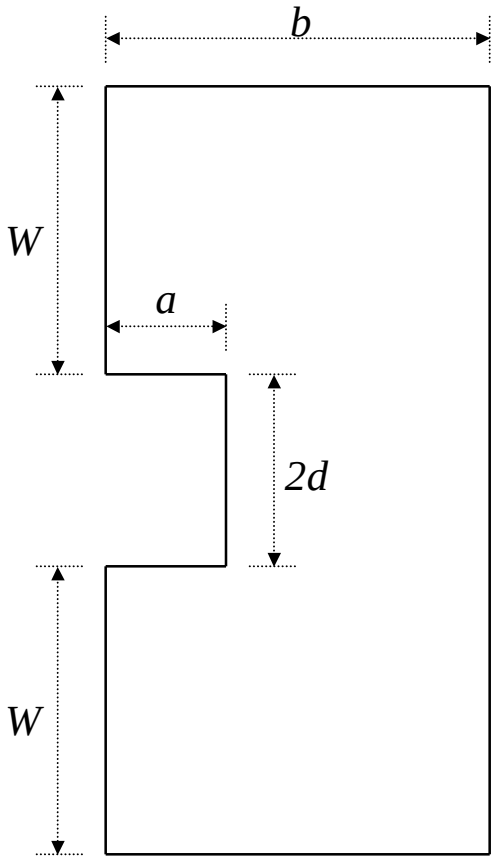


Fig.1b. Schematic representation of the problem considered. (The computational domain in (*r*, *z*) coordinates. *a* and 2*d* are respectively the radius and the length of the particle, *b* is the pore radius, and *W* is a sufficiently large length.)

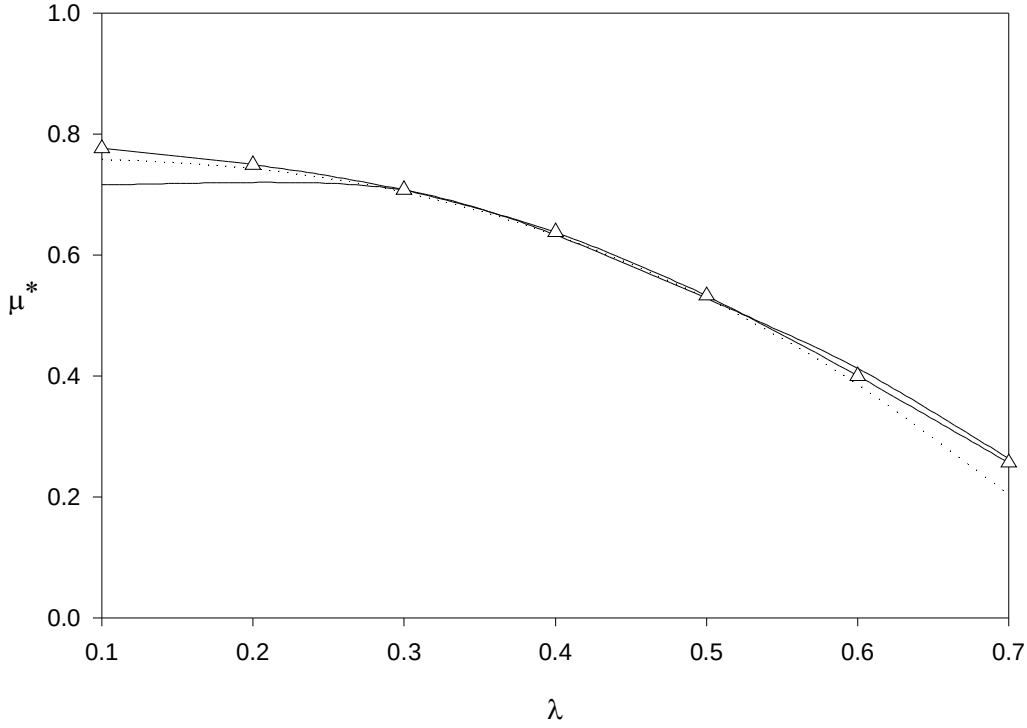


Fig.2. Variation of scaled mobility $\mu^*$ ($=U\eta/\zeta_S E\varepsilon$) as a function of $\lambda$ for the case a sphere of constant surface potential $\zeta_S$ is placed on the axis of an uncharged cylindrical pore. Parameters used are $\kappa a$=4.3, $\zeta_S = k_B T/e$, $T$=298 K, $\eta$=$10^{-3}$ kg/m/s, $\varepsilon$=7.083x$10^{-10}$ C/V/m. $\Delta$, numerical result based on FlexPDE, dashed line, results based on the reflection method of Ennis and Anderson [17], solid line, numerical result of Shugai and Carnie [20].

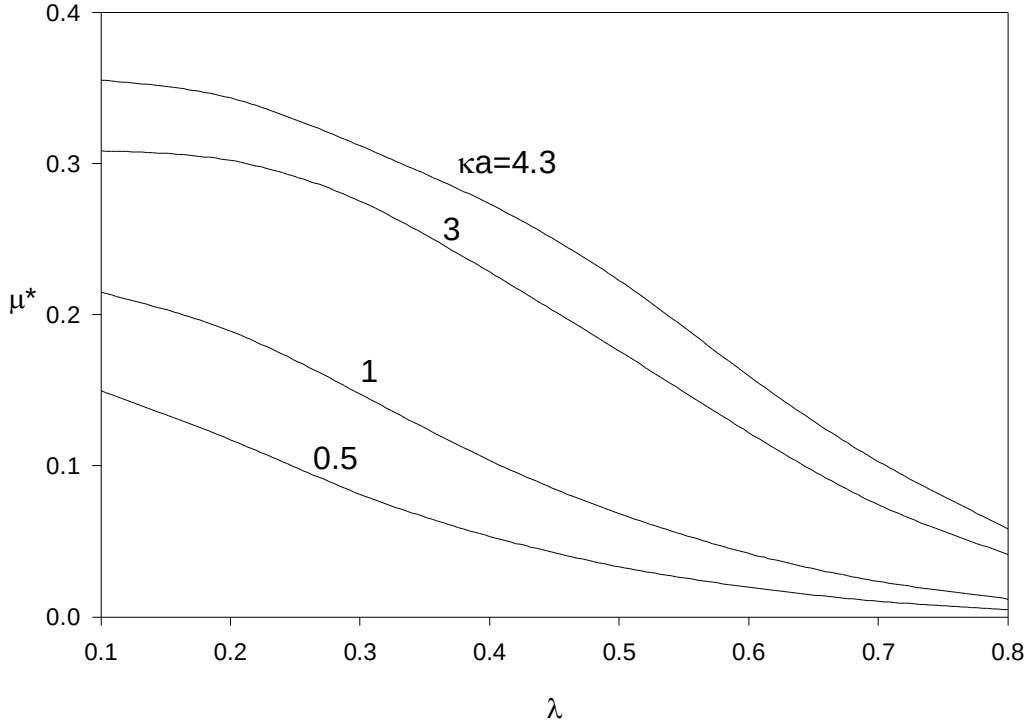


Fig.3a. Variation of scaled electrophoretic mobility $\mu^*$ ($=U\eta/\zeta_{REF}E\varepsilon$) as a function of $\lambda$ ($=a/b$) at various particle aspect ration $a/d$ and $\kappa a$. Parameters used are $\sigma_1 = \sigma_2 = 0.5$ ($\varepsilon\kappa k_B T/e$), $\zeta_{REF} = k_B T/e$, $T$=298 K, $\eta = 10^{-3}$ kg/m/s, $\varepsilon$ =7.083x10$^{-10}$ C/V/m. ($a/d$=1/2)

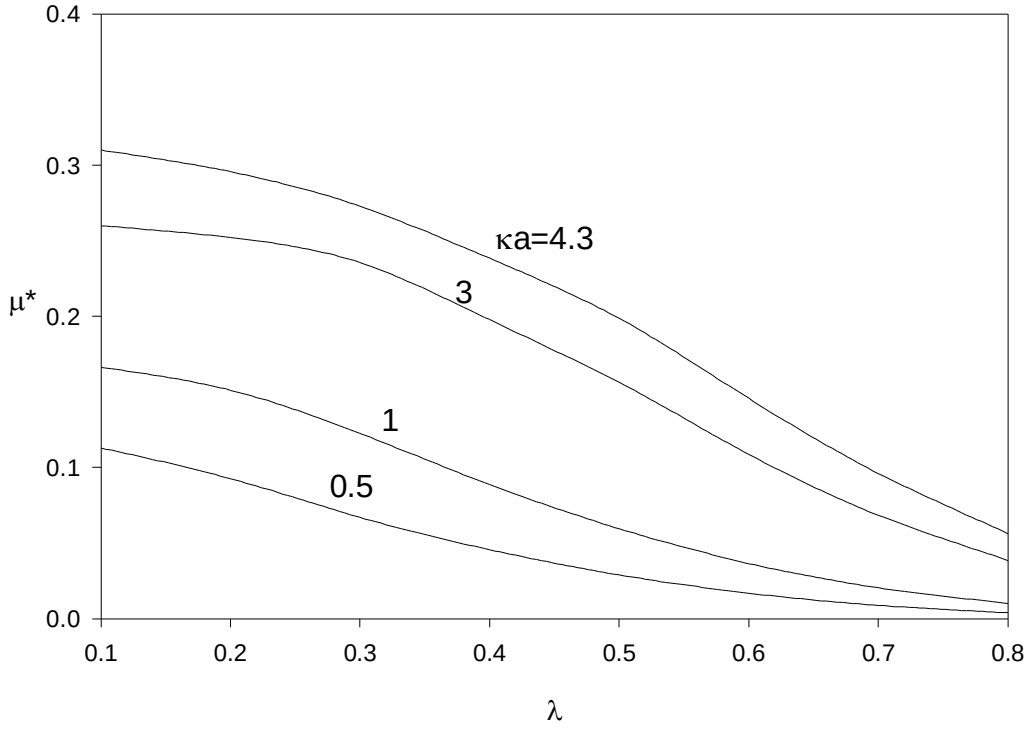


Fig.3b. Variation of scaled electrophoretic mobility $\mu^*$ ($=U\eta/\zeta_{REF}E\varepsilon$) as a function of $\lambda$ ($=a/b$) at various particle aspect ration $a/d$ and $\kappa a$. Parameters used are $\sigma_1 = \sigma_2 = 0.5$ ($\varepsilon\kappa k_B T/e$), $\zeta_{REF} = k_B T/e$, $T$=298 K, $\eta$ =$10^{-3}$ kg/m/s, $\varepsilon$ =7.083x$10^{-10}$ C/V/m. ($a/d$=1)

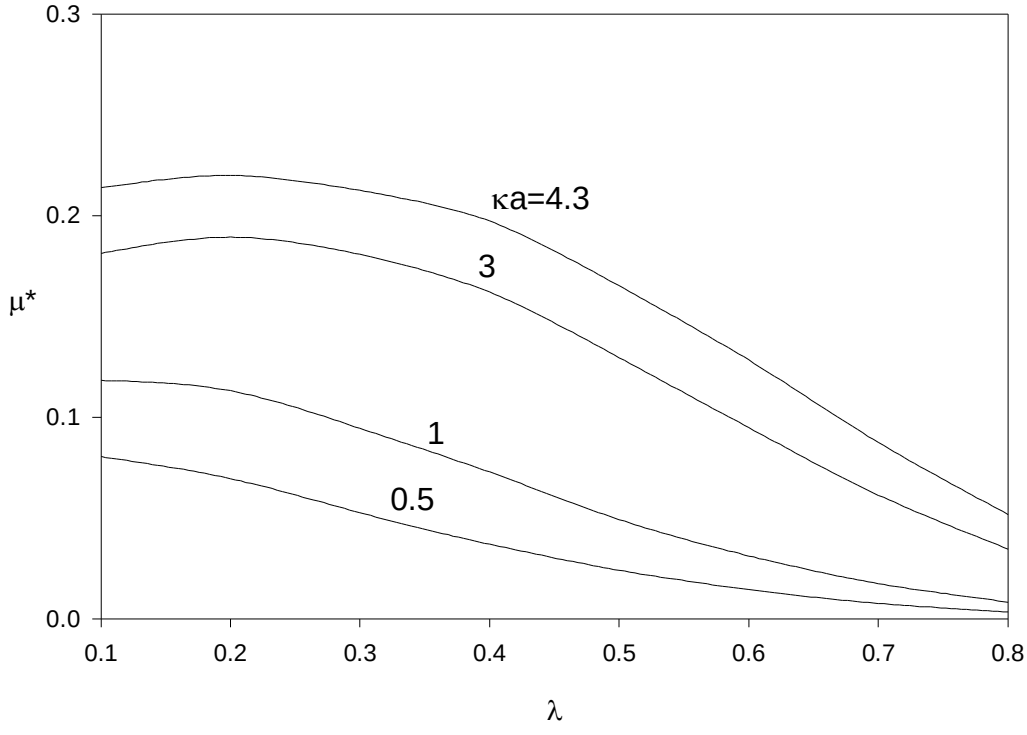


Fig.3c. Variation of scaled electrophoretic mobility $\mu^*$ ($=U\eta/\zeta_{REF}E\varepsilon$) as a function of $\lambda$ ($=a/b$) at various particle aspect ration $a/d$ and $\kappa a$. Parameters used are $\sigma_1 = \sigma_2 = 0.5$ ($\varepsilon\kappa k_B T/e$), $\zeta_{REF} = k_B T/e$, $T$=298 K, $\eta$ =$10^{-3}$ kg/m/s, $\varepsilon$ =7.083x$10^{-10}$ C/V/m. ($a/d$=2)

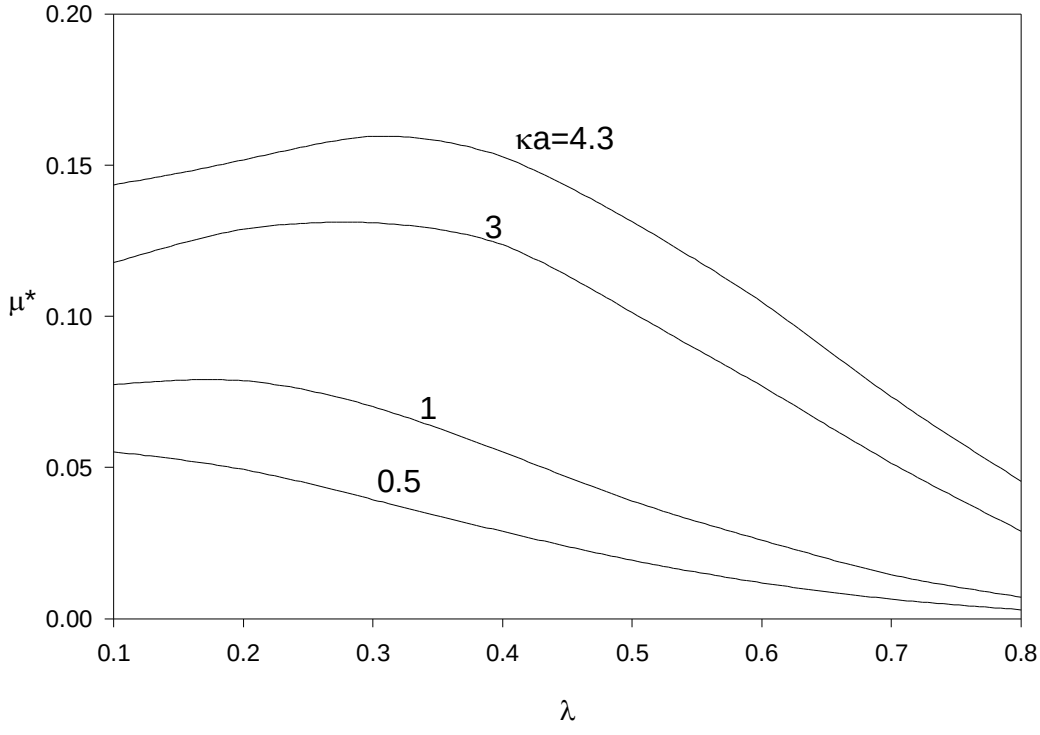


Fig.3d. Variation of scaled electrophoretic mobility $\mu^*$ ($=U\eta/\zeta_{REF}E\varepsilon$) as a function of $\lambda$ ($=a/b$) at various particle aspect ration $a/d$ and $\kappa a$. Parameters used are $\sigma_1 = \sigma_2 = 0.5$ ($\varepsilon\kappa k_B T/e$), $\zeta_{REF} = k_B T/e$, $T$=298 K, $\eta$ =$10^{-3}$ kg/m/s, $\varepsilon$ =7.083x$10^{-10}$ C/V/m. ($a/d$=4)

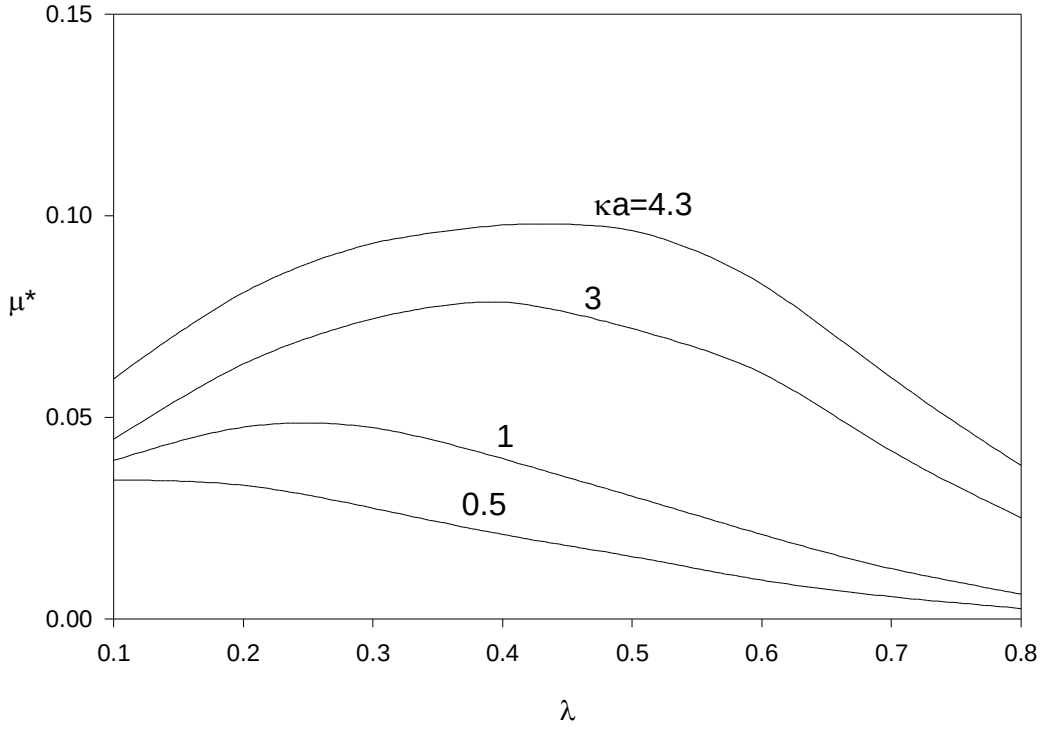


Fig.3e. Variation of scaled electrophoretic mobility $\mu^*$ ($=U\eta/\zeta_{REF}E\varepsilon$) as a function of $\lambda$ ($=a/b$) at various particle aspect ration $a/d$ and $\kappa a$. Parameters used are $\sigma_1 = \sigma_2 = 0.5$ ($\varepsilon\kappa k_B T/e$), $\zeta_{REF} = k_B T/e$, $T$=298 K, $\eta$ =$10^{-3}$ kg/m/s, $\varepsilon$ =7.083x$10^{-10}$ C/V/m. ($a/d$=8)

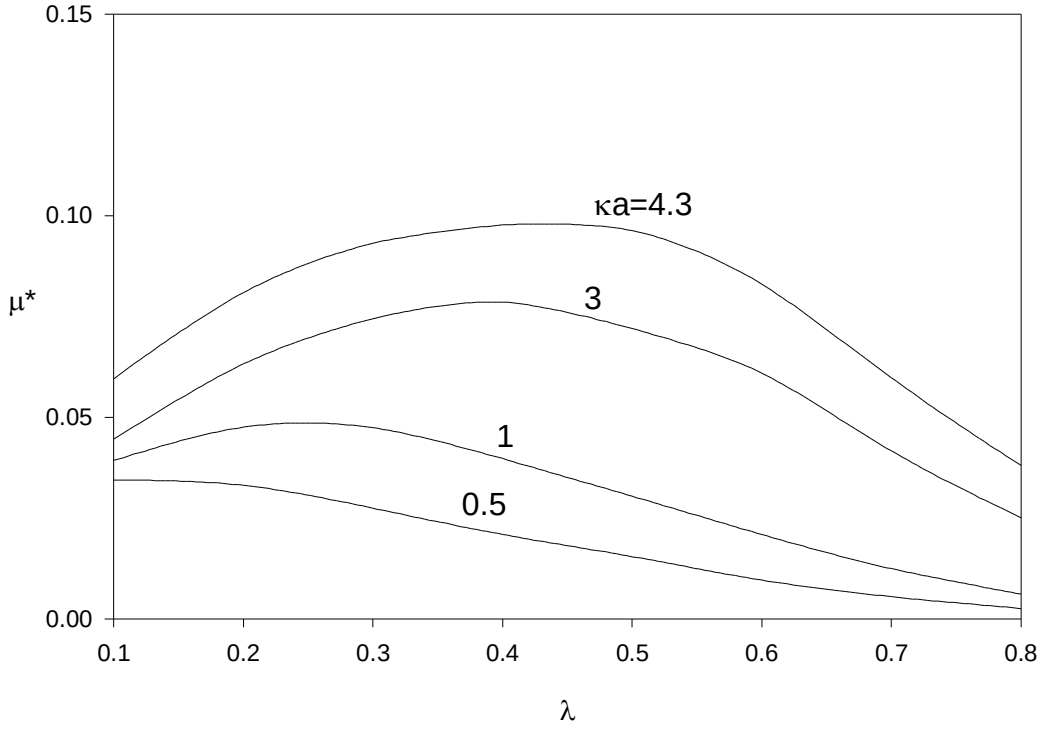


Fig.5.4a. Variation of scaled electrophoretic mobility $\mu^*$ as a function of $\lambda$ for the case of Fig.3 at various particle aspect radio $a/d$ and $\kappa a$. Parameters used are the same as Fig.3 except that $-\sigma_1 = \sigma_2 = 0.5$ ($\varepsilon \kappa k_B T / e$). ($a/d$=1/2)

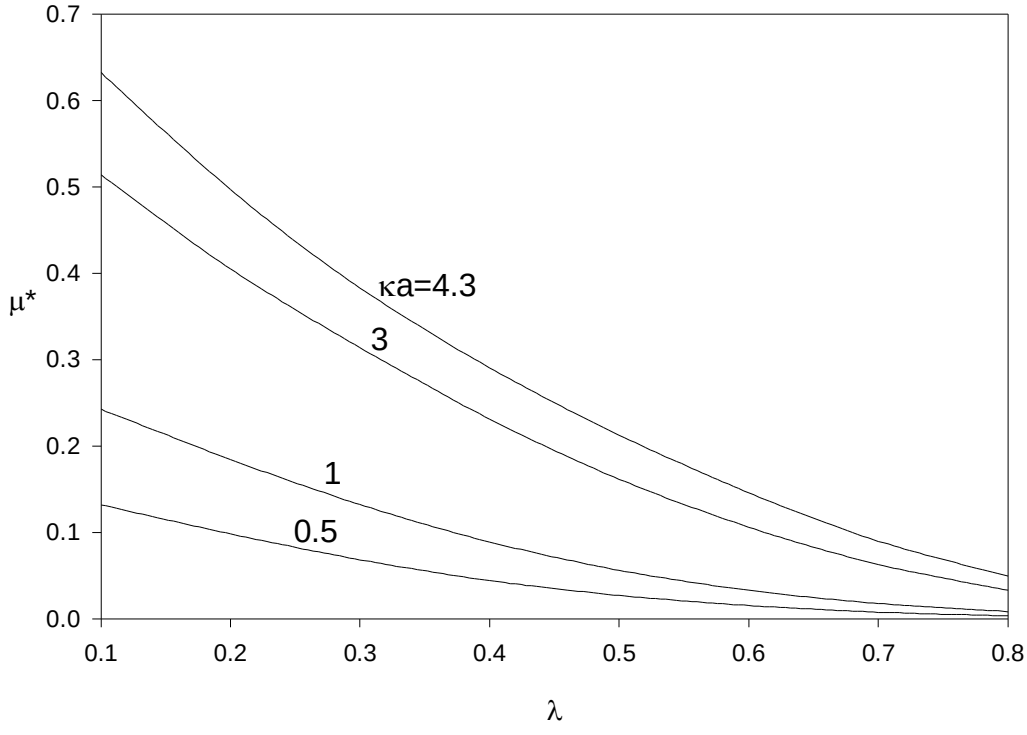


Fig.4b. Variation of scaled electrophoretic mobility $\mu^*$ as a function of $\lambda$ for the case of Fig.3 at various particle aspect radio $a/d$ and $\kappa a$. Parameters used are the same as Fig.3 except that $-\sigma_1 = \sigma_2 = 0.5$ ($\varepsilon \kappa k_B T / e$). ($a/d$=1)

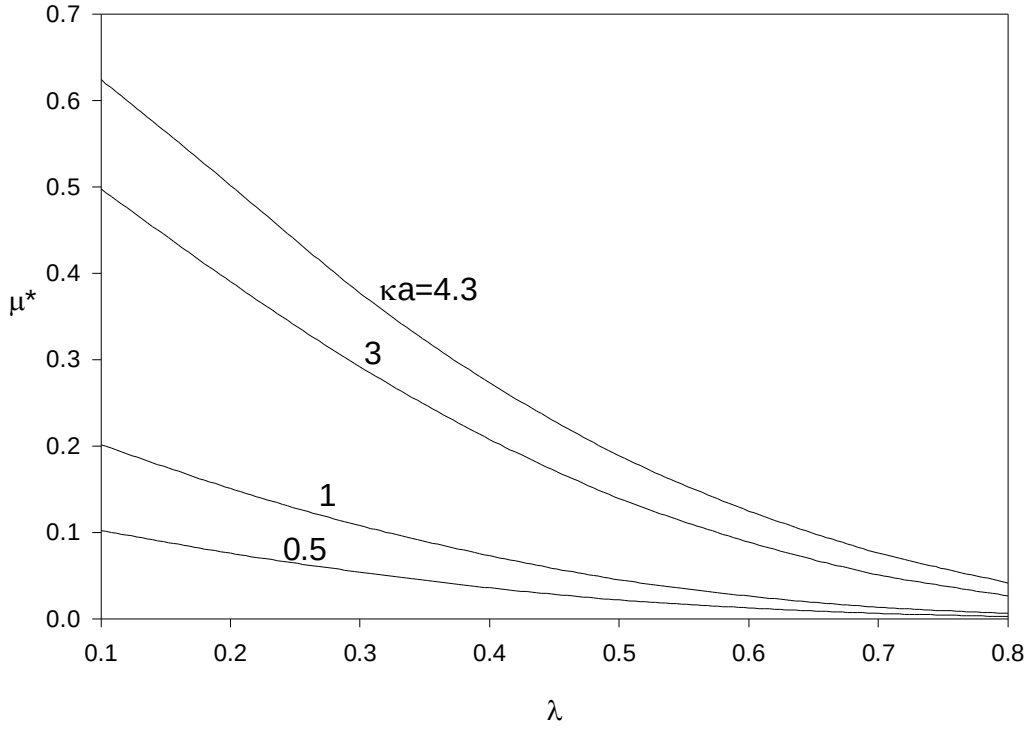


Fig.4c. Variation of scaled electrophoretic mobility $\mu^*$ as a function of $\lambda$ for the case of Fig.3 at various particle aspect radio $a/d$ and $\kappa a$. Parameters used are the same as Fig.3 except that $-\sigma_1 = \sigma_2 = 0.5$ ($\varepsilon\kappa k_B T / e$). ($a/d$=2)

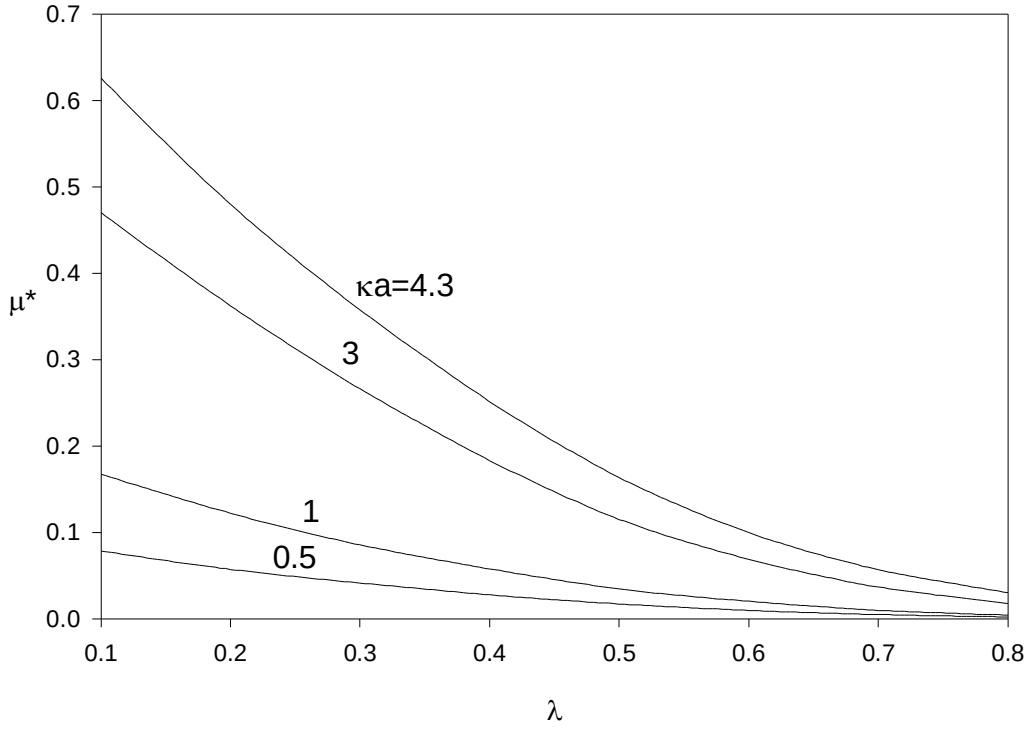


Fig.4d. Variation of scaled electrophoretic mobility $\mu^*$ as a function of $\lambda$ for the case of Fig.5.3 at various particle aspect radio $a/d$ and $\kappa a$. Parameters used are the same as Fig.3 except that $-\sigma_1 = \sigma_2 = 0.5$ ($\varepsilon\kappa k_B T / e$). ($a/d$=4)

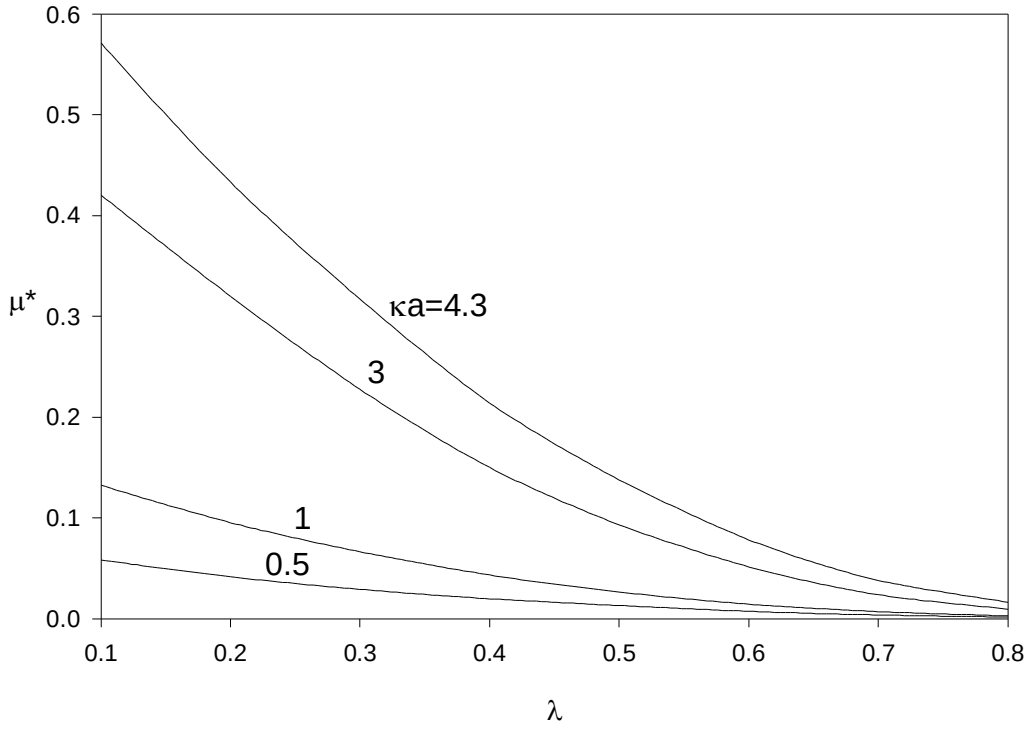


Fig.4e. Variation of scaled electrophoretic mobility $\mu^*$ as a function of $\lambda$ for the case of Fig.3 at various particle aspect ratio $a/d$ and $\kappa a$. Parameters used are the same as Fig.3 except that $-\sigma_1 = \sigma_2 = 0.5$ ($\varepsilon \kappa k_B T / e$). ($a/d$=8)

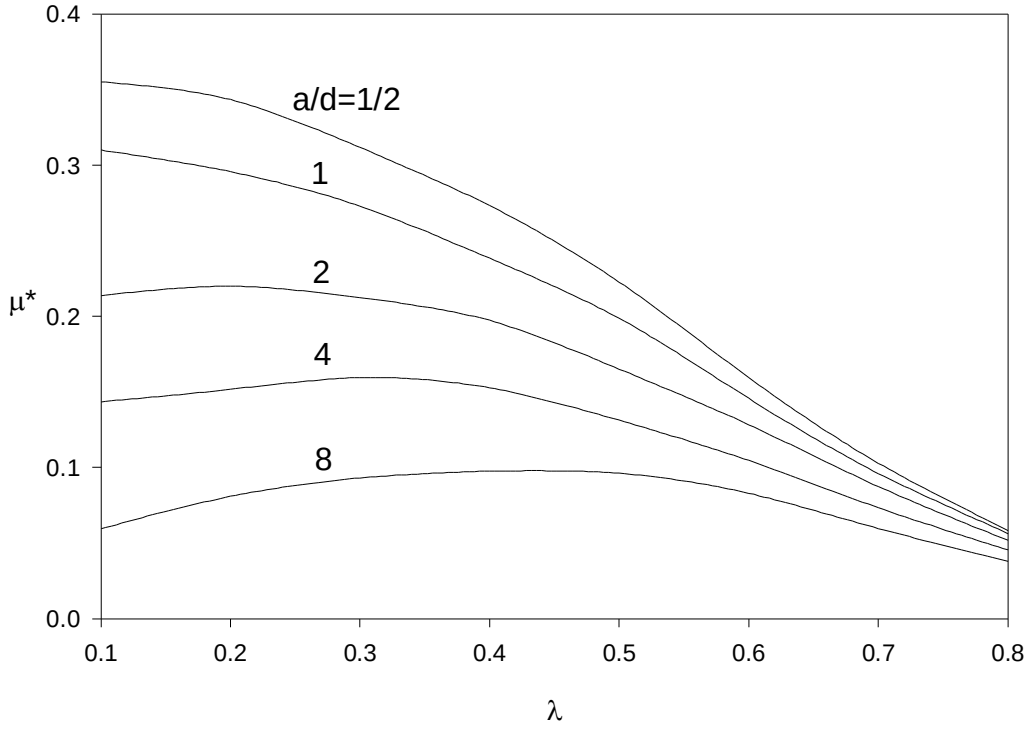


Fig.5a. Variation of scaled electrophoretic mobility $\mu^*$ as a function of $\lambda$ for the case of Fig.3 for various particle aspect ratio ($a/d$) at various particle aspect ratio $a/d$. ($\kappa a = 4.3$)

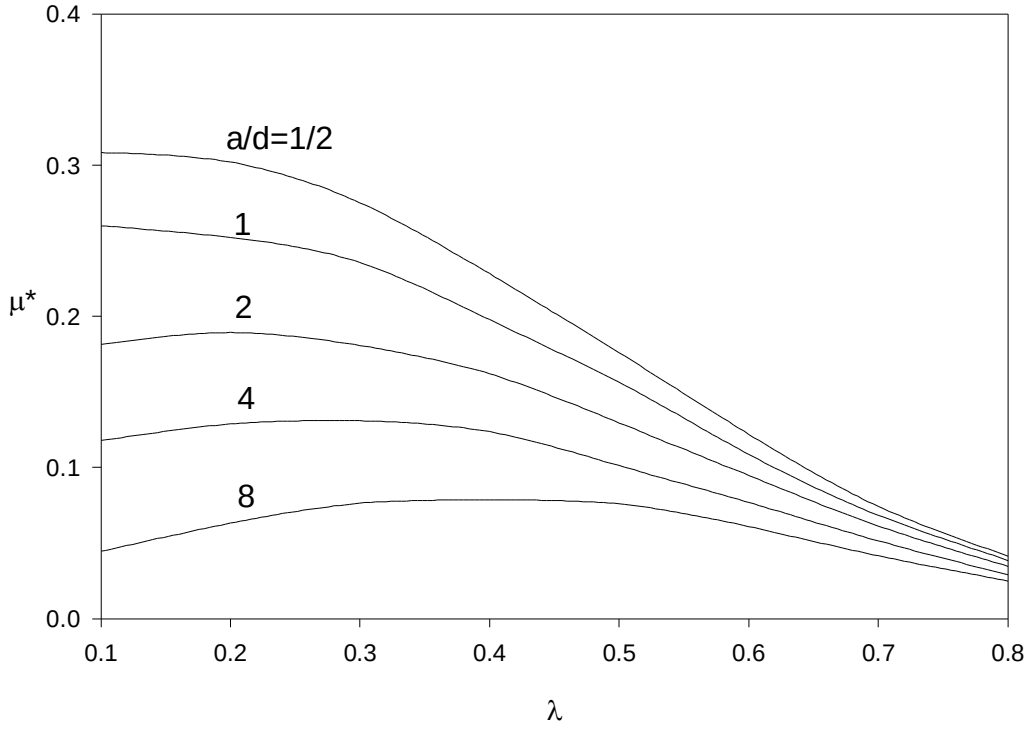


Fig.5b. Variation of scaled electrophoretic mobility $\mu^*$ as a function of $\lambda$ for the case of Fig.3 for various particle aspect ratio ($a/d$) at various particle aspect ratio $a/d$. ($\kappa a = 3$)

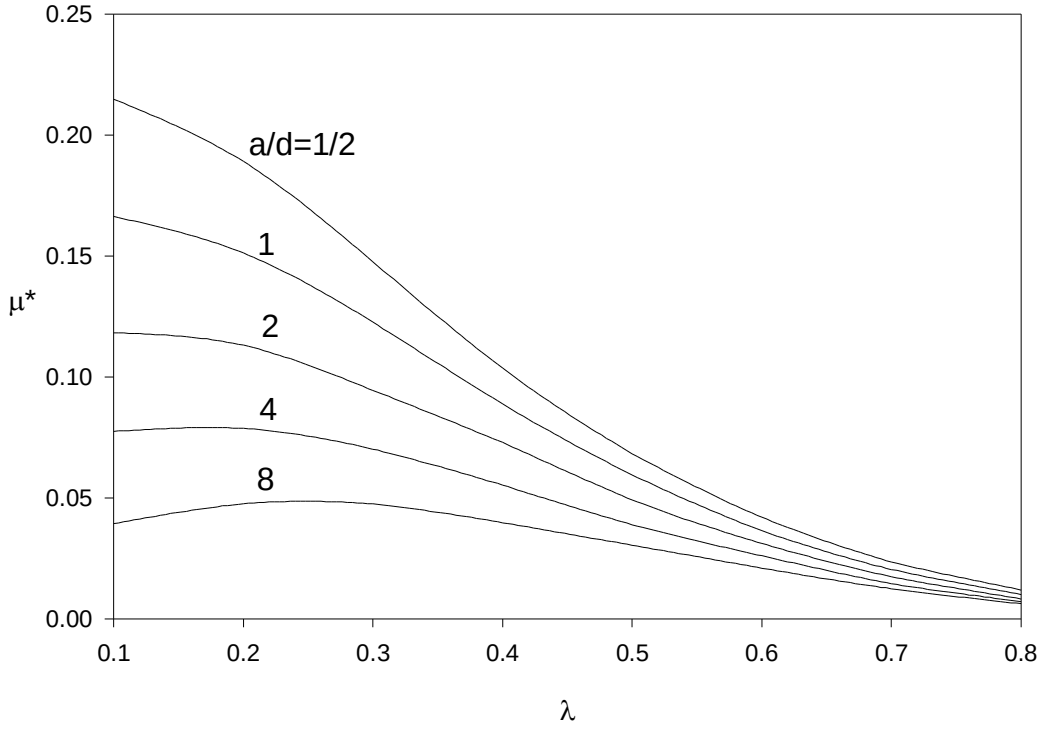


Fig.5c. Variation of scaled electrophoretic mobility $\mu^*$ as a function of $\lambda$ for the case of Fig.3 for various particle aspect ratio ($a/d$) at various particle aspect ratio $a/d$. ($\kappa a = 1$)

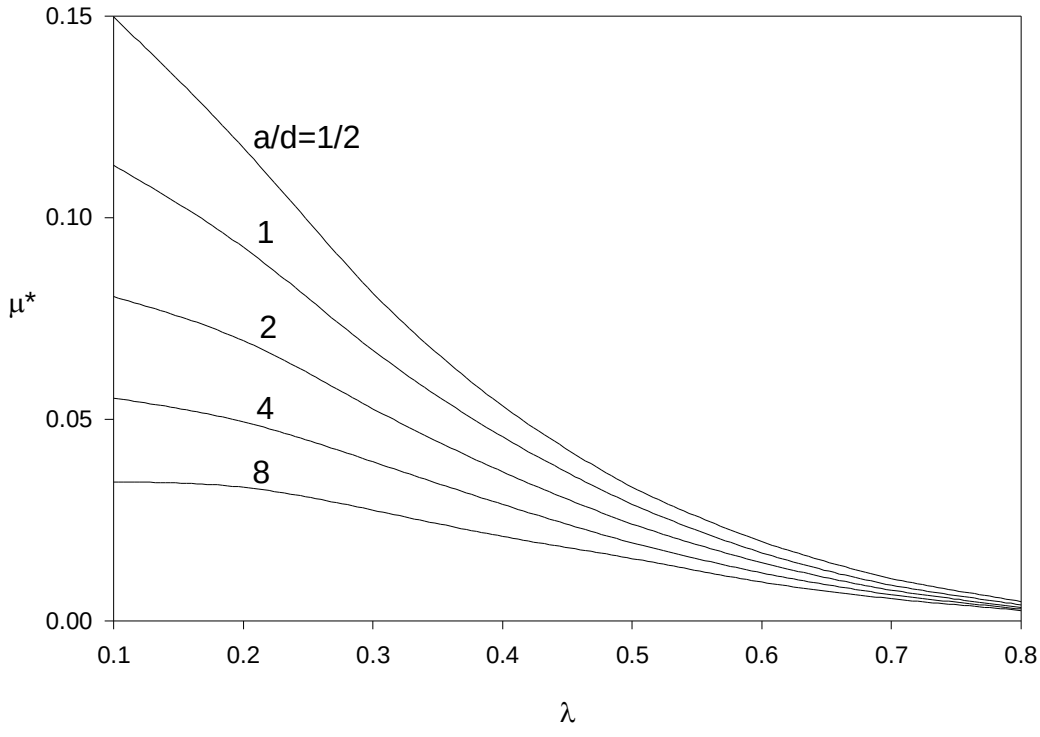


Fig.5d. Variation of scaled electrophoretic mobility $\mu^*$ as a function of $\lambda$ for the case of Fig.3 for various particle aspect ratio ($a/d$) at various particle aspect ratio $a/d$. ($\kappa a = 0.5$)

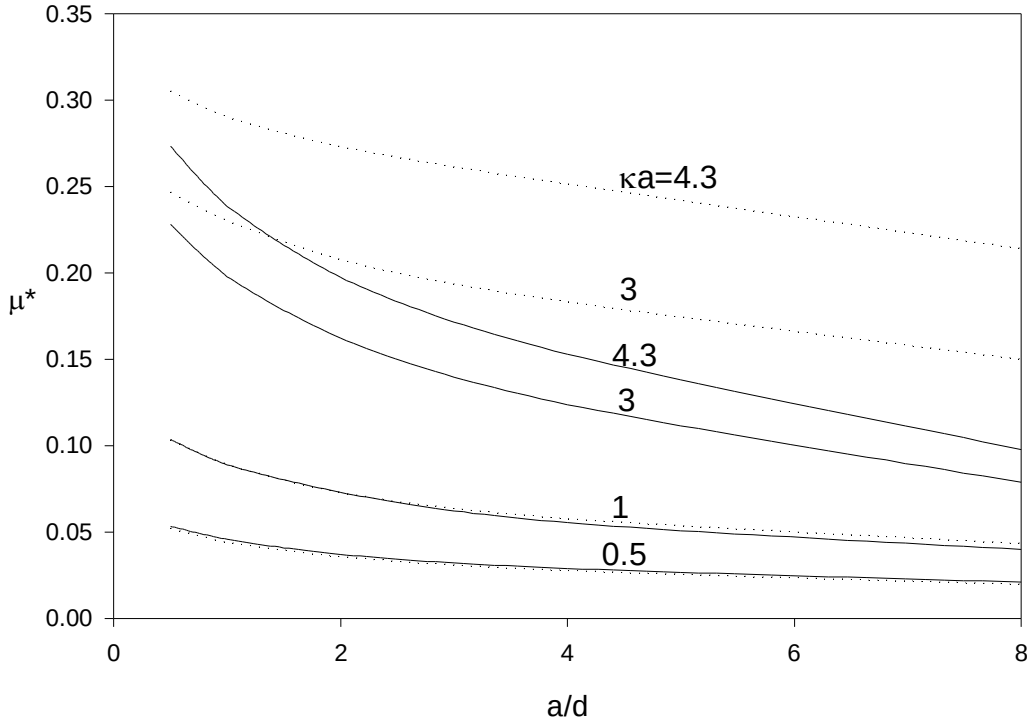


Fig.6. Variation of scaled electrophoretic mobility $\mu^*$ as a function of particle aspect ratio *a/d* for the case of Figs.3 or 4 with $\lambda$ =0.4 for different surface charge density at various $\kappa a$. Solid line $\sigma_1 = \sigma_2$ =0.5 ($\varepsilon\kappa k_B T / e$), dashed line, $-\sigma_1 = \sigma_2$ =0.5 ($\varepsilon\kappa k_B T / e$).

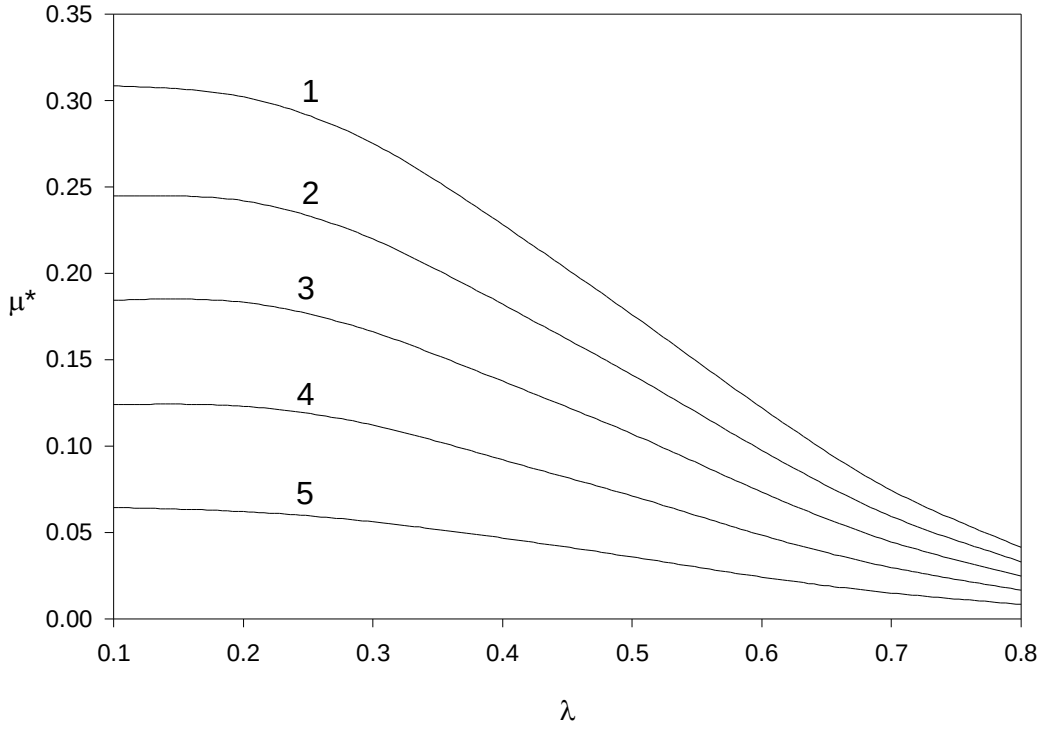


Fig.7a. Variation of scaled electrophoretic mobility $\mu^*$ as a function of $\lambda$ at various surface charge density and particle aspect ratio $a/d$ for the case of Fig.3. Parameters used are: $\kappa a$ =3, $\zeta_{REF} = k_B T / e$, $T$=298 K, $\eta$ =$10^{-3}$ kg/m/s, and $\varepsilon$ =7.083x$10^{-10}$ C/V/m. Curve 1 $\sigma_1 = \sigma_2$=0.5 ($\varepsilon\kappa k_B T / e$); Curve 2, $\sigma_1 = \sigma_2$=0.4 ($\varepsilon\kappa k_B T / e$); Curve 3, $\sigma_1 = \sigma_2$=0.3 ($\varepsilon\kappa k_B T / e$); Curve 4, $\sigma_1 = \sigma_2$=0.2 ($\varepsilon\kappa k_B T / e$); Curve 5, $\sigma_1 = \sigma_2$=0.1 ($\varepsilon\kappa k_B T / e$). ($a/d$=1/2)

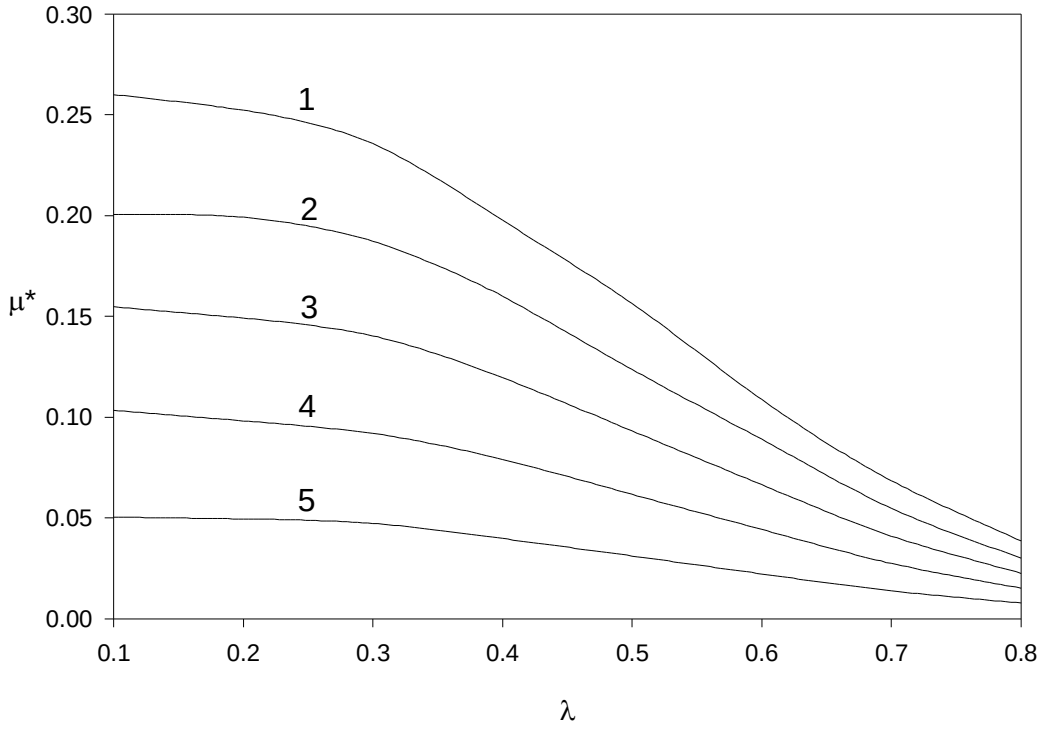


Fig.7b. Variation of scaled electrophoretic mobility $\mu^*$ as a function of $\lambda$ at various surface charge density and particle aspect ratio $a/d$ for the case of Fig.3. Parameters used are: $\kappa a$ =3, $\zeta_{REF} = k_B T / e$, $T$=298 K, $\eta$ =$10^{-3}$ kg/m/s, and $\varepsilon$ =7.083x$10^{-10}$ C/V/m. Curve 1 $\sigma_1 = \sigma_2$=0.5 ($\varepsilon\kappa k_B T / e$); Curve 2, $\sigma_1 = \sigma_2$=0.4 ($\varepsilon\kappa k_B T / e$); Curve 3, $\sigma_1 = \sigma_2$=0.3 ($\varepsilon\kappa k_B T / e$); Curve 4, $\sigma_1 = \sigma_2$=0.2 ($\varepsilon\kappa k_B T / e$); Curve 5, $\sigma_1 = \sigma_2$=0.1 ($\varepsilon\kappa k_B T / e$). ($a/d$=1)

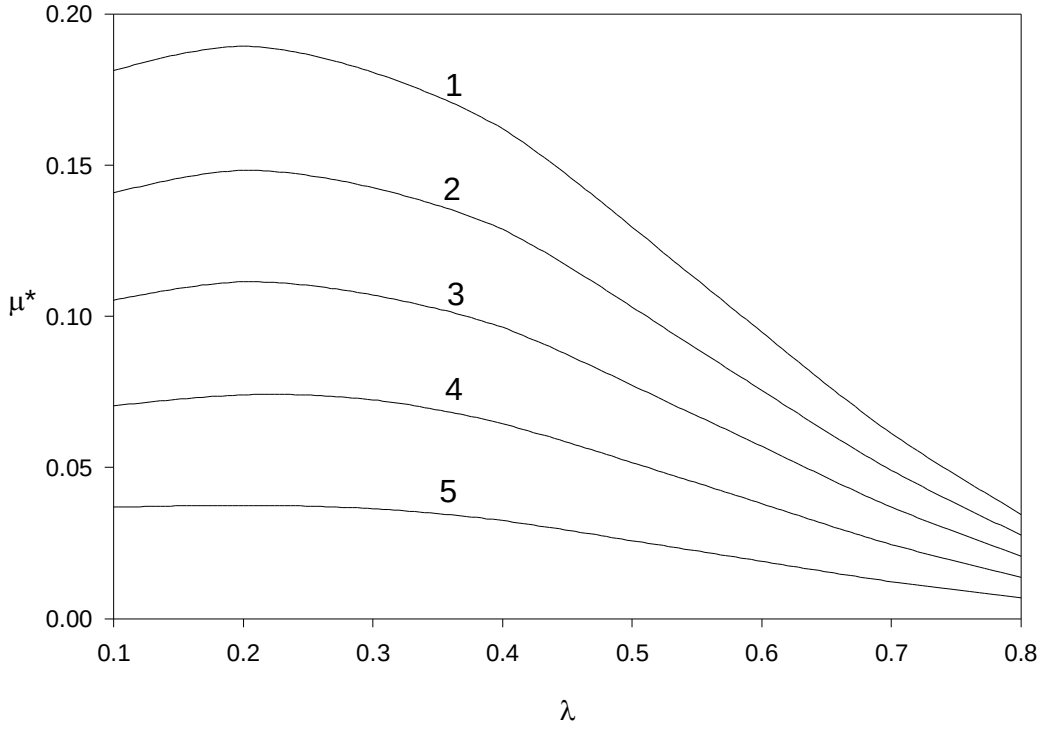


Fig.7c. Variation of scaled electrophoretic mobility $\mu^*$ as a function of $\lambda$ at various surface charge density and particle aspect ratio $a/d$ for the case of Fig.3. Parameters used are: $\kappa a$ =3, $\zeta_{REF} = k_B T / e$, $T$=298 K, $\eta$ =$10^{-3}$ kg/m/s, and $\varepsilon$ =7.083x$10^{-10}$ C/V/m. Curve 1, $\sigma_1 = \sigma_2$=0.5 ($\varepsilon\kappa k_B T / e$); Curve 2, $\sigma_1 = \sigma_2$=0.4 ($\varepsilon\kappa k_B T / e$); Curve 3, $\sigma_1 = \sigma_2$=0.3 ($\varepsilon\kappa k_B T / e$); Curve 4, $\sigma_1 = \sigma_2$=0.2 ($\varepsilon\kappa k_B T / e$); Curve 5, $\sigma_1 = \sigma_2$=0.1 ($\varepsilon\kappa k_B T / e$). ($a/d$=2)

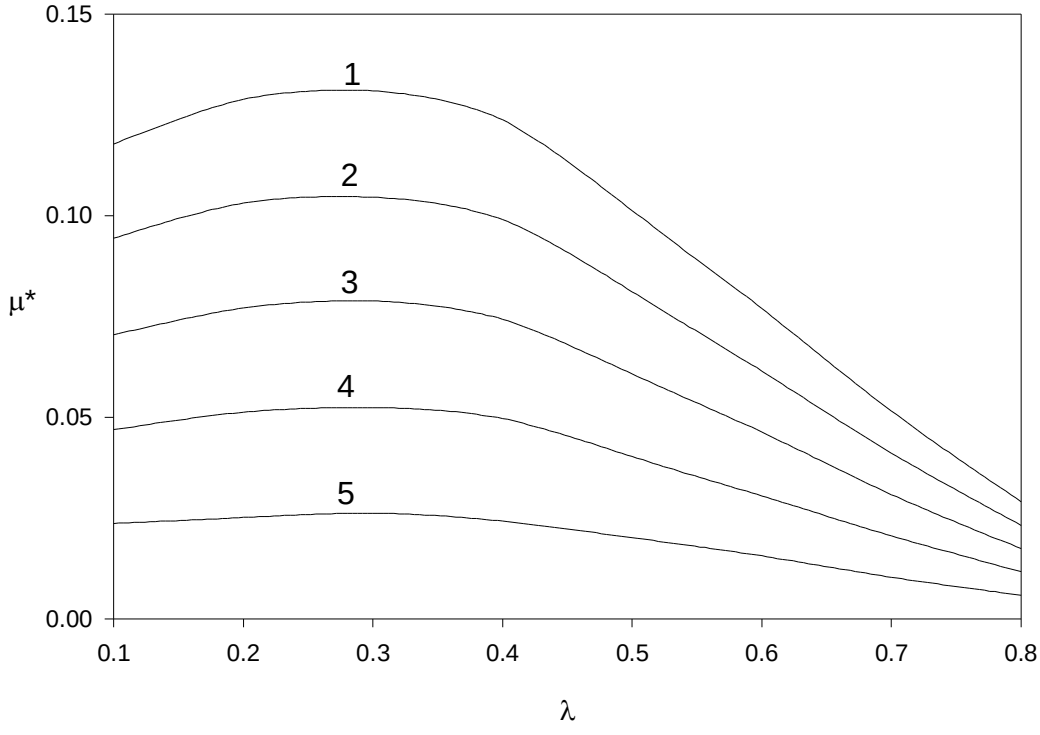


Fig.7d. Variation of scaled electrophoretic mobility $\mu^*$ as a function of $\lambda$ at various surface charge density and particle aspect ratio $a/d$ for the case of Fig.3. Parameters used are: $\kappa a$ =3, $\zeta_{REF} = k_B T / e$, $T$=298 K, $\eta$ =$10^{-3}$ kg/m/s, and $\varepsilon$ =7.083x$10^{-10}$ C/V/m. Curve 1 $\sigma_1 = \sigma_2$=0.5 ($\varepsilon\kappa k_B T / e$); Curve 2, $\sigma_1 = \sigma_2$=0.4 ($\varepsilon\kappa k_B T / e$); Curve 3, $\sigma_1 = \sigma_2$=0.3 ($\varepsilon\kappa k_B T / e$); Curve 4, $\sigma_1 = \sigma_2$=0.2 ($\varepsilon\kappa k_B T / e$); Curve 5, $\sigma_1 = \sigma_2$=0.1 ($\varepsilon\kappa k_B T / e$). ($a/d$=4)

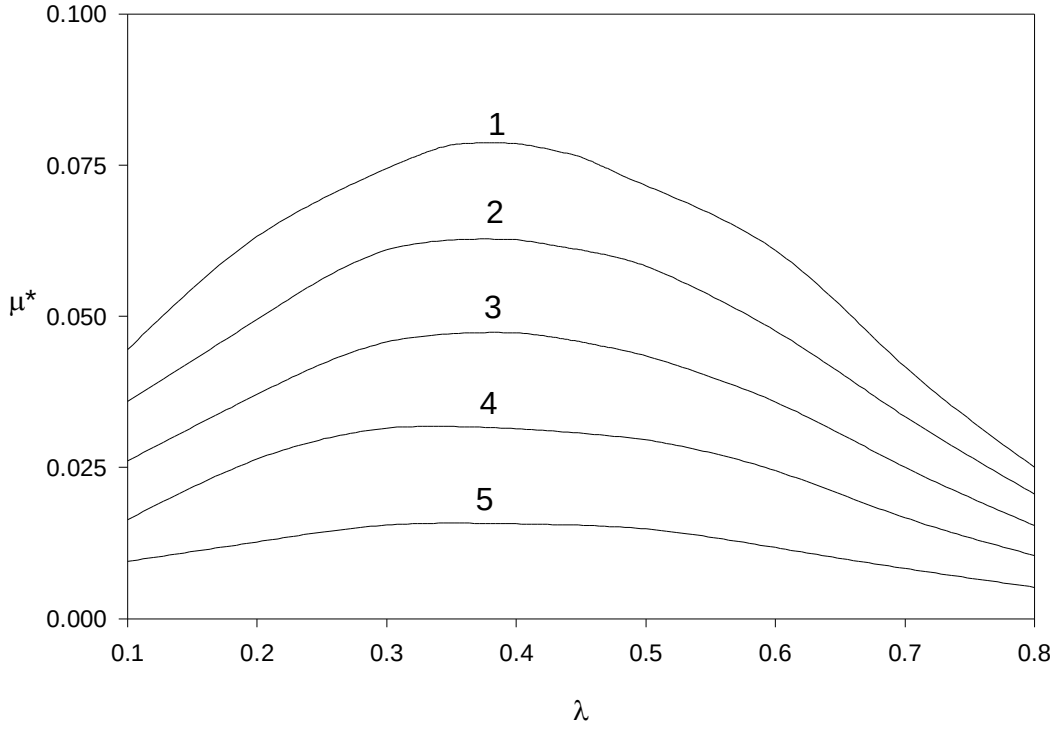


Fig.7e. Variation of scaled electrophoretic mobility $\mu^*$ as a function of $\lambda$ at various surface charge density and particle aspect ratio $a/d$ for the case of Fig.3. Parameters used are: $\kappa a$ =3, $\zeta_{REF} = k_B T / e$, $T$=298 K, $\eta$ =$10^{-3}$ kg/m/s, and $\varepsilon$ =7.083x$10^{-10}$ C/V/m. Curve 1 $\sigma_1 = \sigma_2$=0.5 ($\varepsilon\kappa k_B T / e$); Curve 2, $\sigma_1 = \sigma_2$=0.4 ($\varepsilon\kappa k_B T / e$); Curve 3, $\sigma_1 = \sigma_2$=0.3 ($\varepsilon\kappa k_B T / e$); Curve 4, $\sigma_1 = \sigma_2$=0.2 ($\varepsilon\kappa k_B T / e$); Curve 5, $\sigma_1 = \sigma_2$=0.1 ($\varepsilon\kappa k_B T / e$). ($a/d$=8)

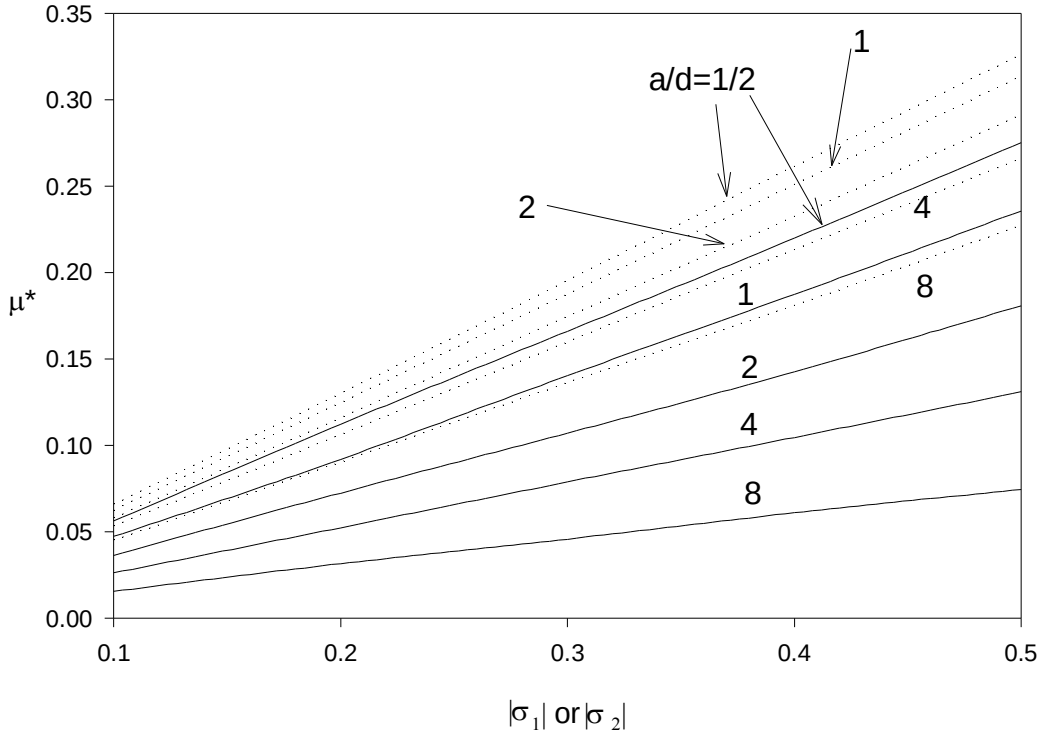


Fig.8. Variation of scaled electrophoretic mobility $\mu^*$ as a function of surface charge density $|\sigma_1|$ (or $|\sigma_2|$) for the case of Fig.3 at two different surface charge densities for various particle aspect ratio *a/d* for the case $\lambda$ =0.3 and $\kappa a$ =3. Solid line: $\sigma_1 = \sigma_2$ =0.5 ($\varepsilon\kappa k_B T / e$); dashed line: $-\sigma_1 = \sigma_2$ =0.5 ($\varepsilon\kappa k_B T / e$).